Low-Level Cloud Response to the Gulf Stream Front in Winter Using *CALIPSO**

JING-WU LIU

Physical Oceanography Laboratory, and Ocean–Atmosphere Interaction and Climate Laboratory, Ocean University of China, Qingdao, China

SHANG-PING XIE

Scripps Institution of Oceanography, University of California, San Diego, La Jolla, California, International Pacific Research Center and Department of Meteorology, School of Ocean and Earth Science and Technology, University of Hawai'i at Mānoa, Honolulu, and Physical Oceanography Laboratory, and Ocean–Atmosphere Interaction and Climate Laboratory, Ocean University of China, Qingdao, China

JOEL R. NORRIS

Scripps Institution of Oceanography, University of California, San Diego, La Jolla, California

SU-PING ZHANG

Physical Oceanography Laboratory, and Ocean–Atmosphere Interaction and Climate Laboratory, Ocean University of China, Qingdao, China

(Manuscript received 6 August 2013, in final form 21 December 2013)

ABSTRACT

A sharp sea surface temperature front develops between the warm water of the Gulf Stream and cold continental shelf water in boreal winter. This front has a substantial impact on the marine boundary layer. The present study analyzes and synthesizes satellite observations and reanalysis data to examine how the sea surface temperature front influences the three-dimensional structure of low-level clouds. The *Cloud–Aerosol Lidar and Infrared Pathfinder Satellite Observations* (*CALIPSO*) satellite captures a sharp low-level cloud transition across the Gulf Stream front, a structure frequently observed under the northerly condition. Low-level cloud top (<4 km) increases by about 500 m from the cold to the warm flank of the front. The sea surface temperature front induces a secondary low-level circulation through sea level pressure adjustment with ascending motion over the warm water and descending motion over cold water. The secondary circulation further contributes to the cross-frontal transition of low-level clouds. Composite analysis shows that surface meridional advection over the front plays an important role in the development of the marine atmospheric boundary layer and low-level clouds. Under cold northerly advection over the Gulf Stream front, strong near-surface instability leads to a well-mixed boundary layer over the Gulf Stream, causing southward deepening of low-level clouds across the sea surface temperature front. Moreover, the front affects the freezing level by transferring heat to the atmosphere and therefore influences the cross-frontal variation of the cloud phase.

1. Introduction

The Gulf Stream is the strongest western boundary current in the ocean transporting heat from the tropics to higher latitudes. A sharp sea surface temperature (SST) front forms between the warm water of the Gulf Stream and cold continental shelf water. The Gulf Stream dramatically influences local weather phenomena. It releases a huge amount of heat to the atmosphere

* International Pacific Research Center Publication Number 1055 and School of Ocean and Earth Science and Technology Publication Number 9114.

Corresponding author address: Jing-Wu Liu, Physical Oceanography Laboratory, and Ocean–Atmosphere Interaction and Climate Laboratory, Ocean University of China, Qingdao, China, 238, Songling Road, Laoshan, Qingdao 266100, China.
E-mail: liujingwu@126.com

DOI: 10.1175/JCLI-D-13-00469.1

in winter (Bane and Osgood 1989), contributing to the explosive cyclogenesis (Sanders and Gyakum 1980; Sanders 1986). Synoptic rainbands are frequently observed along the Gulf Stream axis (Hobbs 1987), and lighting flashes are more frequent and stronger over the Gulf Stream (Biswas and Hobbs 1990).

Recent studies have shown that the Gulf Stream also markedly affects the regional climate. Warm SST produces frequent high surface winds (Sampe and Xie 2007), strong wind speed (O'Neill et al. 2010), and surface wind convergence (Chelton et al. 2004) over the Gulf Stream. Minobe et al. (2008) found that the surface wind convergence anchors a band of rain and upward motion in the annual mean that extends from the boundary layer to the upper troposphere. Minobe et al. (2010) subsequently examined the seasonal cycle of the atmospheric response and found a shallow heating mode of the atmosphere by the Gulf Stream in winter and a deep-heating mode in summer. Numerical models indicate that strong SST gradient results in a deeper marine atmospheric boundary layer (MABL) over the warm water and induces a secondary cross-frontal circulation within the MABL (Huang and Raman 1988; Wai and Stage 1989).

Low-level clouds play an important role in air–sea interaction since they reduce the amount of solar radiation absorbed by the ocean (Wood 2012) and they vary in height and morphology with the stratification of the MABL (Norris 1998a; Tokinaga et al. 2009). The influence of the Gulf Stream on synoptic low-level clouds has been previously reported. Cloud bands often originate at the upwind flank of the Gulf Stream meanders (Young and Sikora 2003). Li et al. (2004) observed a cloud line along the Gulf Stream axis in a satellite image. Similarly, Tokinaga et al. (2009) observed a sharp transition in MABL clouds across the Kuroshio Extension front using laser ceilometers mounted on research vessels. One shortcoming of previous studies is that they were generally based on research cruises or a small number of satellite observations, and the response of low-level clouds to the Gulf Stream on climate time scales remains poorly understood.

The large-scale climatology of marine cloudiness has been previously studied using visual observations from volunteer observing ships. Klein and Hartmann (1993) found that seasonal and interannual variations of low-level stratiform clouds are related to lower-tropospheric static stability. Norris (1998b) studied the global distribution of low-level clouds according to morphological categories and found a north-to-south transition from stratocumulus to cumulus when winds flow equatorward in the western Pacific. Minobe et al. (2010) showed that midlevel cloud occurrence is most frequent right over the Gulf Stream in winter based on the Atmospheric Infrared Sounder and the Advanced Microwave Sounding Unit. Previous climatological studies, however, suffered from coarse spatial resolution and cannot depict variations of low-level clouds across the narrow SST front (about 200–300 km wide).

The *Cloud–Aerosol Lidar and Infrared Pathfinder Satellite Observations* (*CALIPSO*) satellite was launched on 28 April 2006 by the National Aeronautics and Space Administration (NASA) and the French Centre National d'Études Spatiales (CNES) to study the impact of clouds and aerosols on Earth's radiation budget and climate (Winker et al. 2009). A selective, iterated boundary location algorithm is used to detect cloud layers from the lidar backscatter signals (Vaughan et al. 2009). *CALIPSO* provides a cloud-layer product with high spatial resolution. In addition, *CALIPSO* flies in formation with other five satellites [including Advanced Microwave Scanning Radiometer for Earth Observing System (AMSR-E), *CloudSat*, and *Aqua*] in the sun-synchronous A-Train for coincident observations. The combination of the *CALIPSO* lidar, *CloudSat* radar, and Moderate Resolution Imaging Spectroradiometer (MODIS) infrared radiometer (DARDAR, named for radar–lidar instrument combination) provides vertical slices of cloud phase properties along the A-Train tracks (Delanoë and Hogan 2008).

Global and regional cloud structures have been investigated using *CALIPSO* and DARDAR. Nazaryan et al. (2008) studied the spatial and temporal variations of global cirrus based on *CALIPSO*. Bouniol et al. (2012) and Stein et al. (2011) studied the cloud structure in West Africa. Medeiros et al. (2010) found that the vertical distribution of low-level cloud height is consistent with observations from the Rain in Cumulus over the Ocean (RICO) field study. Thus, *CALIPSO* offers the capability of detecting the small-scale structure of clouds.

The present study focuses on how low-level clouds respond to the Gulf Stream from a climate perspective by analyzing *CALIPSO* and synthesizing other satellite observations and reanalysis data. This paper is the first systematic study of SST frontal effects on clouds with direct observations by a cloud-top height instrument in space. Taking advantage of a high-resolution and multiyear record of observations, we investigate how low-level clouds vary across the SST front in winter. We also use the European Centre for Medium-Range Weather Forecasts (ECMWF) Interim Re-Analysis (ERA-Interim) to examine the MABL structure corresponding to cross-frontal variations of low-level clouds. Since the direction of meridional surface winds is important for the low-level atmospheric stability, we apply composite

analysis according to the surface meridional winds. Our results serve as a template to study cloud transition near other strong SST fronts.

2. Data

a. Temporal and spatial domains

We employ a suite of high-resolution satellite observations and reanalysis data during the five winters (December of 2006–10, January and February of 2007–11) when the observations of *CALIPSO*, *CloudSat*, and AMSR-E overlap. The December–February (DJF) climatology in the present study is defined as the average values during this period. Note that the Quick Scatterometer (QuikSCAT) is available from July 1999 to November 2009, and does not perfectly overlap with *CALIPSO*. We refer to QuikSCAT averaged in DJF between 1999 and 2009 as a climatology. The spatial domain of the composite analysis is roughly 30°–50°N, 65°–50°W where the Gulf Stream flows nearly eastward.

b. Satellite observations

We use the *CALIPSO* cloud layer product (http://www-calipso.larc.nasa.gov/; Winker et al. 2009) to investigate low-level cloud structure. Details on the retrieval algorithms can be found in Vaughan et al. (2009). The spatial resolution of the *CALIPSO* cloud layer product is 1 km in the horizontal and 30 m in the vertical below 8.5 km. *CALIPSO* provides up to 10 cloud-top heights per profile, and the highest cloud tops below 4 km are considered to be the low-level cloud top (LCT) following the algorithm of Zhang et al. (2012), who investigated cloud-top heights near Hawaii. It should be noted that *CALIPSO* observes low-level clouds only when the higher clouds are not optically thick. This is not a problem for the present study because low-level clouds are dominant near the Gulf Stream in winter (not shown). Since this paper focuses on marine clouds, *CALIPSO* profiles over land are omitted. *CALIPSO* passes the Gulf Stream region around 0500 and 1600 UTC (0000 and 1100 local time). Orbital tracks pass over the same location at the same local time every 16 days.

We also use the DARDAR-MASK that combines *CloudSat*, *CALIPSO*, and MODIS (http://www.icare.univ-lille1.fr/projects/dardar/; Delanoë and Hogan 2010) to examine the cloud phase properties. The DARDAR-MASK returns a range of cloud categories: rain, supercooled liquid water, liquid water, ice, and mixed ice and supercooled liquid water. The resolution of DARDAR-MASK is 1.5 km in the horizontal and 240 m in the vertical. We use DARDAR-MASK data to investigate the occurrence of the different cloud categories in the Gulf Stream region. Delanoë et al. (2013) compared airborne in situ, airborne radar–lidar, and DARDAR retrievals of polar ice cloud properties and found that the combination of radar and lidar provides better retrievals than do standalone methods using just the lidar or radar. Further validation of DARDAR with direct measurements would help reduce the uncertainties of DARDAR.

The AMSR-E sensor on the *Aqua* satellite measures SST, surface wind speed, liquid water path (LWP; vertically integrated atmospheric water vapor), and rain rate (Hilburn and Wentz 2008). The AMSR-E data are available from Remote Sensing Systems on a 0.25° × 0.25° grid (http://www.remss.com/). We use AMSR-E SST to locate the position of the Gulf Stream front and use AMSR-E LWP to investigate the relationship between LWP and LCT. *CALIPSO*, *CloudSat*, and *Aqua* are three members of the A-Train satellite constellation that closely follow each other in orbit such and observe the same location within 45 s. The nearly coincident measurements permit the combined analysis of *CALIPSO*, *CloudSat*, and AMSR-E.

In addition, DJF-averaged surface wind velocity and divergence are calculated from daily QuikSCAT observations on a 0.25° × 0.25° grid (Liu 2002; http://www.remss.com/). We calculate the DJF climatology to examine the pattern of surface wind convergence/divergence associated with the Gulf Stream front.

c. Reanalysis data

We use the 6-hourly ERA-Interim fields on a 0.75° × 0.75° grid provided by ECWMF (Dee et al. 2011). ERA-Interim is the latest global atmospheric reanalysis to replace the 40-yr ECMWF Re-Analysis (ERA-40). There are 12 vertical levels below 700 hPa, capable of characterizing MABL features across the SST front. We use ERA-Interim at 0600 and 1800 UTC, which are close to the times of *CALIPSO* observations. The ERA-Interim fields are composited on LCT occurrence to investigate the MABL structure corresponding to the cross-frontal transition of low-level clouds.

d. Precipitation product

The Global Precipitation Climatology Project (GPCP) is used to depict the rainband associated with the Gulf Stream in DJF. We construct 5-yr (December of 2006–10, January and February of 2007–11) DJF-averaged precipitation based on daily GPCP data on a 1° × 1° grid.

3. Winter climatology

The Gulf Stream flows along the North American coast, separates from the coast at Cape Hatteras, and continues to flow northeastward. The sharp SST front

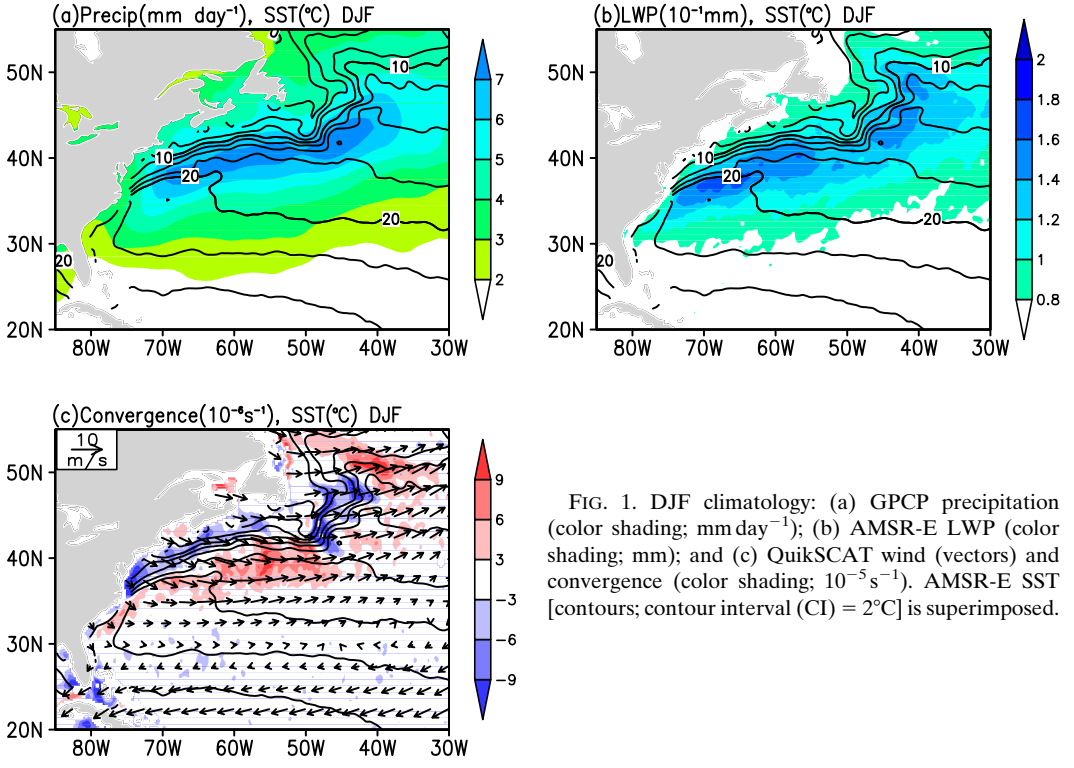

FIG. 1. DJF climatology: (a) GPCP precipitation (color shading; mm day^{-1}); (b) AMSR-E LWP (color shading; mm); and (c) QuikSCAT wind (vectors) and convergence (color shading; 10^{-5} s^{-1}). AMSR-E SST [contours; contour interval (CI) = 2°C] is superimposed.

between the warm Gulf Stream water and cold continental shelf water is most developed in winter (Minobe et al. 2010). Across the front, SST increases by 12°C within 400 km, and the SST gradient is sharpest between 40° and 42°N (Fig. 1).

Figure 1a shows that the Gulf Stream anchors a prominent rainband in winter on the southern side of the SST front. Precipitation in the rainband exceeds 7 mm day^{-1}, consistent with the results from the Tropical Rainfall Measuring Mission (Minobe et al. 2010). AMSR-E LWP also exhibits a cloud band over the warm water of the Gulf Stream, collocated with the rainband (Fig. 1b). It should be noted that AMSR-E LWP excludes ice clouds.

The formation of the rainband and cloud band is related to surface wind convergence (Minobe et al. 2008) possibly via the sea level pressure (SLP) adjustment of Lindzen and Nigam (1987). Low-level air temperature adjusts to an SST front through the cross-frontal changes of sensible and latent heat flux, resulting in small-scale SLP variations and upward motion over the warm flank of the SST front and high SLP and downward motion over the cold flank. Minobe et al. (2010) found that the diabatic heating and the upward motion over the warm water are confined to the lower troposphere in winter, implying that the cross-frontal transition is more evident in low-level clouds than higher clouds.

Indeed, the cross-frontal transition of LCT is sharp. Figures 2a and 2b show LCT averaged within 0.5° intervals along the daytime and nighttime *CALIPSO* tracks over the western North Atlantic during winter. Our composites include about 28 *CALIPSO* passes along each track over the averaging period. LCT is lower than 1.4 km on the cold flank of the SST front but rises to 2.4 km over the Gulf Stream. Along the 46°N latitude line where the Gulf Stream flows northeastward, LCT is about 2.2 km at 40°W but only 1.4 km at 48°W, suggesting that the SST front exerts a strong influence on LCT. In general, LCT is higher at night, indicative of a deeper MABL. This is because the entrainment is strengthened by infrared radiation cooling at cloud top at night, but solar radiation weakens this effect in the day. The enhanced entrainment helps deepen MABL (Caldwell et al. 2005). Farther to the south away from the Gulf Stream, the gradual southward decrease of LCT from 35°N is due to large-scale subsidence of the subtropical high. For simplicity, we analyze *CALIPSO* and DARDAR data within the dashed quadrilaterals in which the Gulf Stream flows nearly eastward.

4. Composites of low-level cloud top

a. CALIPSO *low-level cloud top*

Figure 3a shows the zonally averaged DJF climatology of SST, SST minus surface air temperature (SST − SAT),

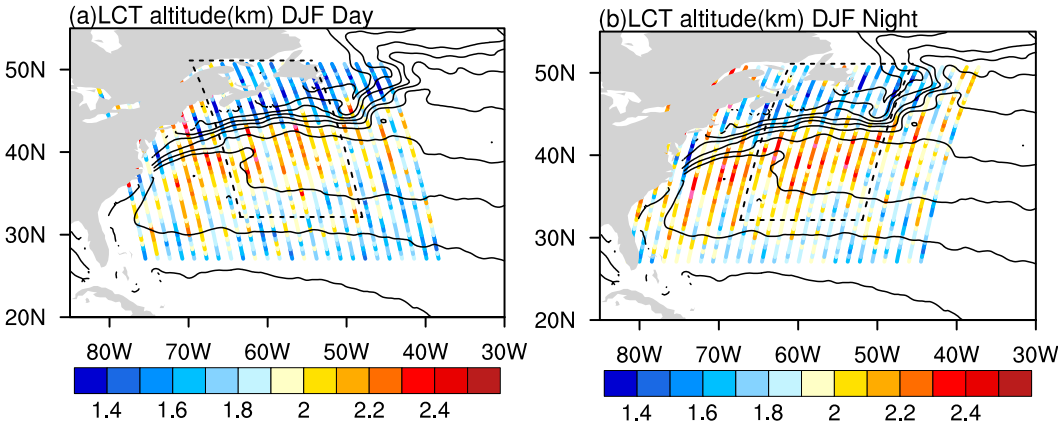

FIG. 2. DJF LCT altitude (color lines; km) along *CALIPSO* tracks during the (a) day and (b) night with AMSR-E SST (contours; CI = 2°C) superimposed. The dashed quadrilaterals indicate the spatial domain of *CALIPSO* and DARDAR composites in subsequent figures.

meridional atmospheric circulation, and virtual potential temperature within the dashed quadrilaterals in Fig. 2. The SST front of the Gulf Stream is sharpest between 41° and 42.5°N (Fig. 3a, bottom) where the prevailing winds are westerly in winter. The westerly jet is 7.2 m s^{-1} at 38°N (not shown), and the meridional wind is weakly southerly over the SST front in the wintertime mean. The SST − SAT maxima are about 5.3° and 4.0°C over the Gulf Stream and near 50°N (Fig. 3a, bottom), respectively. The former peak of SST − SAT is because the atmospheric adjustment to the SST front is slower than the increase of SST when the MABL is advected by the northerly wind from the cold to the warm water. The latter peak reflects the huge surface air temperature contrast between the ocean and continent in winter (Young and Sikora 2003). SST − SAT is an important parameter for lower-tropospheric stability and its spatial pattern is similar to the potential temperature difference

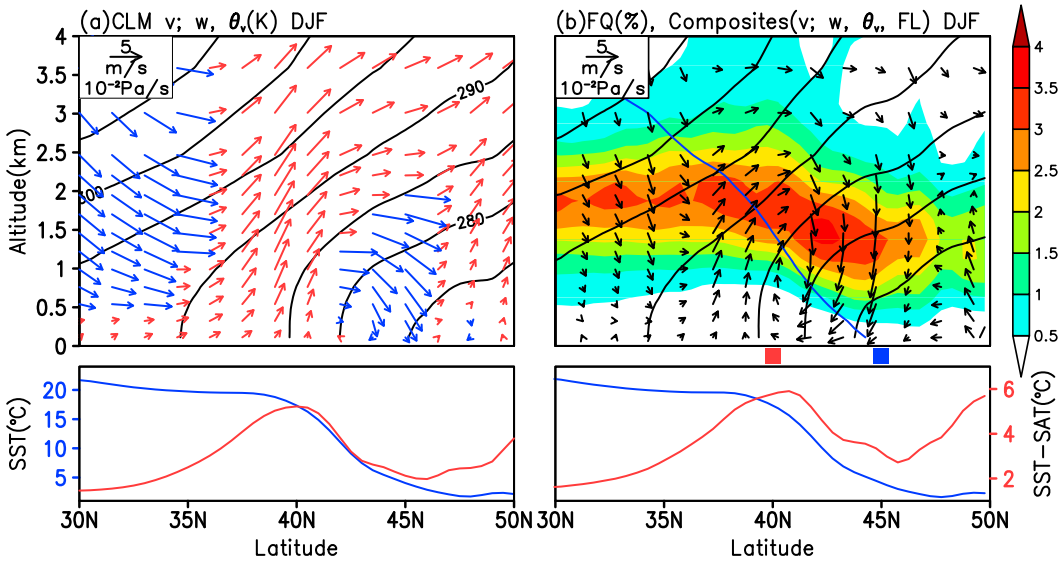

FIG. 3. (a) Zonal mean DJF climatology along *CALIPSO* tracks within the quadrilaterals in Fig. 2 from ERA-Interim: virtual potential temperature (contours; CI = 5 K), meridional wind (m s^{-1}) and vertical velocity (10^{-2} hPa s^{-1}) vectors, SST (blue line in bottom panel; °C), and SST − SAT (red line in bottom panel; °C). The red and blue vectors in the top panel of (a) denote upward motion and downward motion, respectively. (b) The relative frequency of LCT observed by *CALIPSO* as a function of latitude and height (color shading; %). Composite virtual potential temperature (contours; CI = 5 K), meridional wind (m s^{-1}) and vertical velocity (10^{-2} hPa s^{-1}) vectors are constructed according to LCT occurrence. The blue line in the top panel indicates the freezing level where the air temperature is 0°C. The red and blue filled squares in (b) indicate the warm and cold regions used in Figs. 4 and 6.

between 700 and 1000 hPa (not shown), an important parameter for the stratocumulus formation (Wood 2012).

Although the large-scale motion is generally upward between 37° and 50°N, the secondary circulation induced by the SST front is apparent (Fig. 3a). The ascending motion is enhanced over the warm flank of the SST front and weakened over the cold flank, with descending motion between 42° and 45°N below 2.0 km. This is consistent with the surface convergence/divergence based on QuikSCAT (Fig. 1c) according to the continuity equation. Such a secondary circulation in MABL is more evident after applying spatial high-pass filtering (not shown).

Virtual potential temperature is relatively uniform in the vertical below 0.8 km, indicative of a well-mixed MABL (Fig. 3a, top). Closer examination suggests that the MABL is shallower over the cold SST. The vertical gradient of virtual potential temperature is greater between 1- and 1.5-km elevation on the cold flank of the SST front, implying the frequent occurrence of temperature inversions capping MABL. Similarly, near the Kuroshio Extension in winter, the near-surface instability (SST − SAT) effect on the low-level atmospheric structure is obvious in observations (Tokinaga et al. 2009). The lower atmosphere features a well-defined surface mixed layer under unstable conditions, whereas no surface mixed layer is observed in stable conditions.

Figure 3b shows the relative frequency of LCT occurrence as a function of latitude and altitude based on *CALIPSO*. In this case, the ERA-Interim fields (SST − SAT, vertical and meridional winds, virtual potential temperature, and the freezing level) are averaged only when LCT is reported by *CALIPSO*. The relative frequency is calculated using 0.5° bins in the meridional and 0.25-km bins in the vertical. ERA-Interim is interpolated along the *CALIPSO* tracks in 0.5° meridional intervals. An ERA-Interim profile in a 0.5° meridional bin contributes to the average if the bin contains at least 5 out of about 50 *CALIPSO* profiles that report LCTs.

The relative frequency of LCT occurrence exhibits large cross-frontal variations (Fig. 3b). The altitude with most frequent LCT is 1.3 km over the cold flank of the SST front and rises to 1.8 km over the warm flank. Although an SST − SAT maximum and upward motion occur between 48° and 50°N, LCT occurrence is less frequent since the air is dry near the coast. *CALIPSO* is not able to detect the morphological categories of clouds, but Norris and Iacobellis (2005) documented that stratocumulus is prevalent under cold advection over SST gradient in the midlatitude North Pacific. The relative frequency of LCT gradually declines southward from 37°N where the MABL is much shallower, suggesting the breakup of stratocumulus.

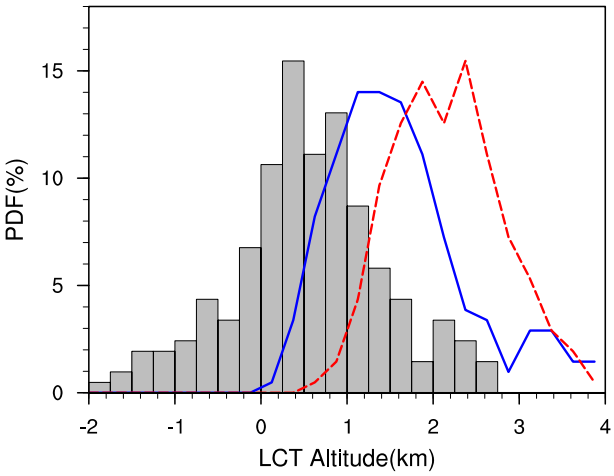

FIG. 4. PDFs (%) of LCT in two regions: 0.5° bins centered at 40°N (red dashed line) and 45°N (blue solid line) along the *CALIPSO* tracks. The gray bars show the PDF of LCT differences between the two regions (40°N minus 45°N) when the LCTs are observed in the two regions along one single track.

The cross-frontal cloud transition is related to the secondary atmospheric circulation in the MABL induced by the SST front below 3 km (Fig. 3b, top). Downward motion occurs below 3 km over the cold flank of the SST front. The frequent occurrence of a temperature inversion over the cold SST confines most low-level clouds below 1.8 km. On the warm flank of the SST front, the composite upward motion is strongest at 2 km, consistent with the altitude of LCT occurrence. In contrast to the mean state (Fig. 3a), stronger surface northerly wind occurs with LCT occurrence north of 40°N (Fig. 3b), suggesting that the cross-frontal transition of low-level clouds is more prevalent under surface northerlies. The composite surface northerly wind is strongest at the center of the SST front in agreement with the QuikSCAT results near the Kuroshio Extension (Tokinaga et al. 2009). Convergence of meridional surface wind over the warm SST is responsible for the ascending motion in the MABL.

Figure 4 further clarifies the cross-frontal transition of LCT, showing the probability density functions (PDFs) of transient LCT altitudes over the warm and cold water and their difference (warm minus cold). The regions of warm and cold water are defined as 0.5° bins centered at 40° and 45°N along the *CALIPSO* tracks, respectively. LCT is most frequent in 1.1–1.7 km over the cold SST but in 1.9–2.5 km over the Gulf Steam. About 50% of the time, the transient LCT at 40°N is at least 0.5 km higher than at 45°N. Similar results are obtained if we exclude all the profiles with clouds above 4 km (not shown).

The influence of the Gulf Stream on clouds might penetrate above the MABL and reach the midtroposphere.

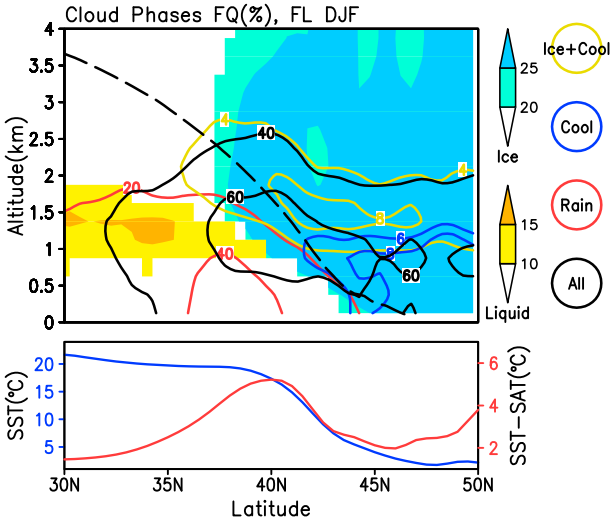

FIG. 5. Zonal mean of frequencies (%) of DARDAR cloud phases: all phases (black contours), ice (blue shading), liquid water (yellow shading), supercooled liquid water (blue contours), rain (red contours), and mixed ice and supercooled liquid water (yellow contours) clouds. The long dashed line indicates the freezing level. The blue and red lines in the bottom panel represent the same SST and SST − SAT in Fig. 3a, respectively.

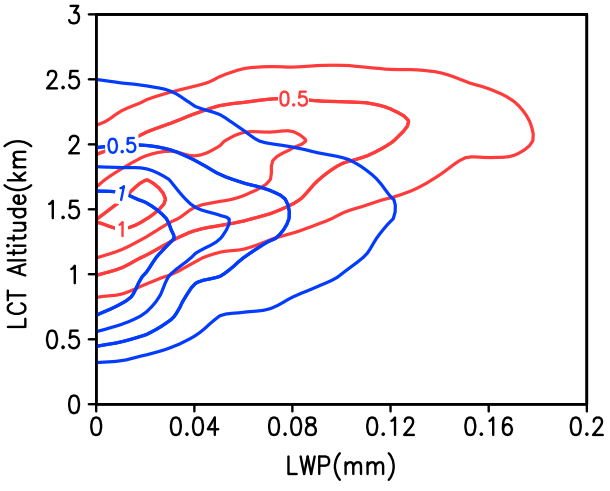

FIG. 6. Joint PDFs of LWP and LCT in two regions: 0.5° bins centered at 45°N (blue contours; CI = 0.25%) and 40°N (red contours; CI = 0.25%) along *CALIPSO* tracks.

The occurrence of cloud top above 4 km is more frequent over the warm water (not shown), supporting the results of Minobe et al. (2010) using Atmospheric Infrared Sounder and the Advanced Microwave Sounding Unit and Tokinaga et al. (2009) over the western North Pacific. We focus on low-level clouds, however, since the cross-frontal transition below 4 km is more evident.

b. *DARDAR cloud categories*

Figure 5 shows cross-frontal transects of cloud phase categories from DARDAR. The frequency of a cloud category occurrence is calculated using same bins as the relative frequency of LCT occurrence. The altitude with the most frequent cloud occurrence (about 60%) is 0.9 km over the cold flank of the SST front, and it reaches up to 1.7 km over the warm flank, indicative of a cross-frontal structure. The categories of liquid and rain dominate below 2.0 km over the warm water. Liquid clouds are more frequent above 1.2 km, while rain class is most frequent below 0.9 km over the Gulf Stream, supporting the horizontal patterns of AMSR-E LWP and GPCP precipitation in winter (Fig. 1). In contrast, ice clouds dominate above the freezing level. Ice clouds found above MABL in the free troposphere (not shown) are as a result of storms. Additionally, the category of supercooled liquid water is mainly confined below 1.5 km over the cold flank of the SST front. The categories of mixed ice and supercooled liquid water are frequently observed near the LCT and rise with the freezing level going southward. The SST front affects the freezing level by transferring heat to the atmosphere and, therefore, influences the cross-frontal variations of cloud categories.

c. *Relationship between* CALIPSO *LCT and AMSR-E LWP*

Figure 6 shows the joint PDFs of *CALIPSO* LCT and AMSR-E LWP over the warm and cold flanks of the SST front, in the 0.5° bins centered at 40° and 45°N along *CALIPSO* tracks, respectively. Assuming that most LWP is confined in the lower atmosphere, it is plausible that larger LWP is associated with higher LCT due to greater physical cloud thickness. This is consistent with the increase in LCT altitude with larger LWP. As LWP increases from 0 to 0.08 mm, LCT increases by 0.8 km over the Gulf Stream (red contours) and by 0.3 km over cold water (blue contours), implying a higher correlation between LWP and LCT over warm water. The lower correlation over the cold water might be due to the frequent occurrence of ice clouds (Fig. 5) that are not included in AMSR-E LWP. Additionally, nearly all low clouds are confined below 2.5 km, which is the upper limit of the MABL in this region (not shown).

5. Northerly and southerly composites

Since the direction of the meridional surface wind is important for near-surface stability, the ERA-Interim fields, the relative frequency of LCT occurrence, and frequencies of cloud categories are calculated separately for surface northerly and southerly regimes. Winds between 40° and 45°N are northerly (southerly) 54.7% (45.3%) of time, and the northerly and southerly

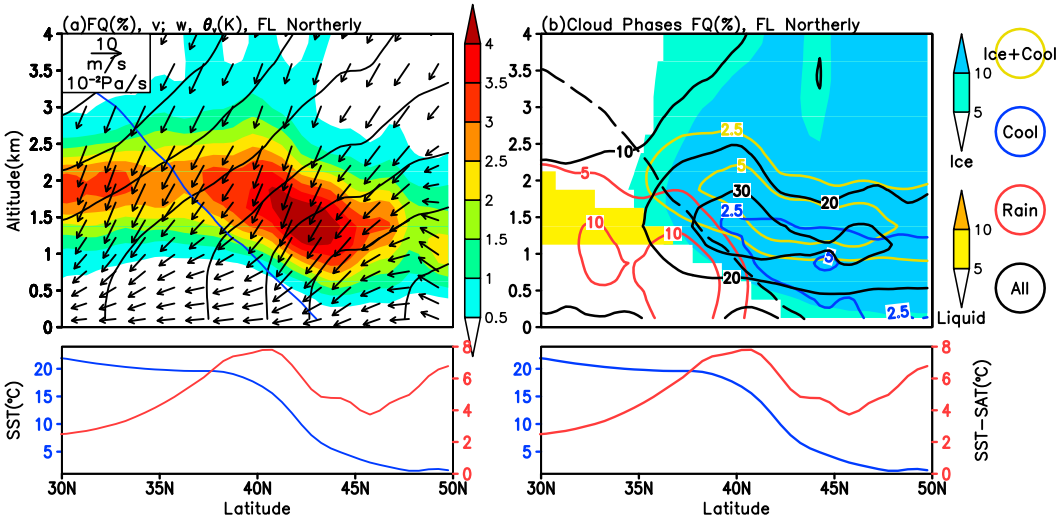

FIG. 7. (a) The relative frequency of LCT (color shading; %) and virtual potential temperature (contours; CI = 5 K), meridional wind ($m\,s^{-1}$), and vertical velocity (10^{-2} hPa s^{-1}) vectors under northerly conditions are composited on the transient meridional surface winds along *CALIPSO* tracks. (b) As in Fig. 5, but for composites under northerly and conditions according to meridional surface winds along *CALIPSO* tracks.

composites include 55 054 and 36 170 LCT observations between 40° and 45°N, respectively.

a. Northerly wind composite

Figures 7a and 7b show the patterns of relative frequency of LCT and frequencies of different cloud categories under conditions of northerly wind reported at 10 m at the time and location of each satellite observation. These resemble the all-condition composites (Figs. 3b and 5) since LCT occurs most frequently under northerly conditions. LCT is elevated over the Gulf Stream where SST − SAT exceeds 6.0°C. Upon close inspection, the cross-frontal transition of relative LCT frequency is more evident than is the case in the all-condition composites because of a stronger inversion produced by large-scale subsidence over the cold flank of the SST front (Fig. 7a). Although the synoptic northerlies are strong, the impact of the SST front on vertical motion is visible. The large-scale descending motion is weakened over the warm flank of the SST front and intensified over the cold flank. The strong surface northerlies lead to high SST − SAT of 8.0° and 6.5°C over the Gulf Stream and the coastal region (Fig. 7a, bottom), much higher than the mean-state and all-conditions composites (Figs. 3a,b). The resulting MABL is more well mixed under cold advection. Small et al. (2003) reported that horizontal advection displaces the SAT response 100 km downwind of the SST forcing in the region of Pacific tropical instability waves where the background winds are approximately 10 $m\,s^{-1}$. A shorter length scale of the SAT adjustment to SST perturbations is expected since the cross-frontal winds are 7 $m\,s^{-1}$ in the northerly composite.

In winter, the Gulf Stream front is under the North American trough where the prevailing winds are westerly (Fig. 8a) and is located in the storm track domain where the synoptic variability is strong. To identify the specific synoptic conditions corresponding to the cross-frontal transition of low-level clouds, the relative frequency of LCT (not shown) and ERA-Interim (Fig. 8b) composites are constructed when the area mean (between 40° and 45°N along the *CALIPSO* tracks) of surface meridional winds is northerly. This calculation differs from Fig. 7a, which is composited on occurrence of surface northerlies at the *CALIPSO* footprint. The relative frequency of LCT is similar to the Fig. 7a (not shown), suggesting that the cross-frontal transition of low-level clouds is robust. Figure 8b shows that cross-frontal northerlies related to the transition of low-level clouds occur after low-pressure systems pass by. The resulting cold advection intensifies heat and moisture flux out of the ocean to the atmosphere, and thus favors the formation of stratocumulus (Young and Sikora 2003).

b. Southerly wind composite

Under southerly conditions, low-level clouds show more complex structures since the entire atmosphere is influenced by synoptic large-scale ascent (Fig. 9a). In contrast to northerly conditions, the MABL is stabilized by warm advection as warm air flows over colder water. The most frequent LCT occurs near 37°N at 1.8 km and

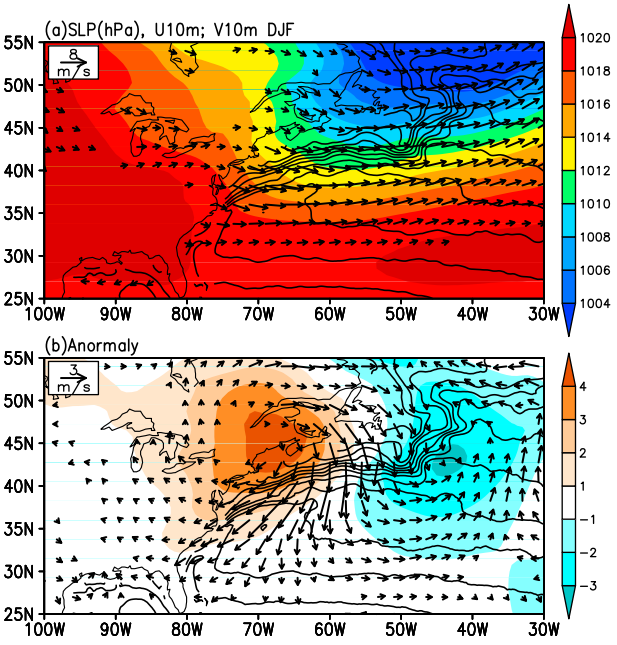

FIG. 8. (a) The DJF ERA-Interim climatology: SLP (color shading; hPa) and sea surface wind velocities (vectors; m s^{-1}). (b) The composite anomalies of SLP (color shading; hPa) and sea surface wind velocities (vectors; m s^{-1}). The composites are constructed according to the occurrence of mean northerly wind between 40° and 45°N along *CALIPSO* tracks. The wind speeds less than 2 and 0.4 m s^{-1} in (a) and (b) are omitted, respectively.

the maximum frequency of rain category is collocated with large SST − SAT, although the near-surface instability is much weaker than under northerly conditions (Fig. 9b). This suggests that the Gulf Stream deepens clouds under the southerly flow and is consistent with the argument of Norris and Iacobellis (2005) that precipitation and nimbostratus are more frequent under regions of strong upward and poleward flow. There is a general northward decrease in temperature in balance with the westerly thermal wind while the SST front maintains a sharp temperature gradient near the surface. Compared to the northerly composite, the freezing level is about 1 km higher at 40°N and occurs 5° poleward at 1-km altitude.

6. Seasonal cycle

The present study focused on the low-level cloud response to the Gulf Stream in winter when the SST front is sharpest, but low-level clouds vary markedly with seasons (Fig. 10). The seasonal variations of low-level clouds (Fig. 10) are closely related to the annual cycle of near-surface stability (Fig. 11). LCT is highest in winter and lowest in summer. In contrast to wintertime conditions, the strong southerly wind brings warm air over the relatively cold ocean during summer, thus stabilizing the surface layer. LCT frequently occurs below 1 km in summer, implying the frequent occurrence of sea fog. These results based on *CALIPSO* are consistent with the visual observation from ships (Norris and Iacobellis 2005). Similarly, Li and Zhang (2013) observed a northward cross-SST-frontal transition from stratus to fog in the East China and Yellow Seas in summer. The relative frequency of LCT peaks over the SST front in winter but over the Gulf Stream in spring. This is because the Gulf Stream is the only heat source during cold-air outbreaks whereas SST − SAT is lower than 1°C north of 43°N in spring (Fig. 10b, bottom) because of the weak springtime thermal contrast between the land and ocean (Young and Sikora 2003).

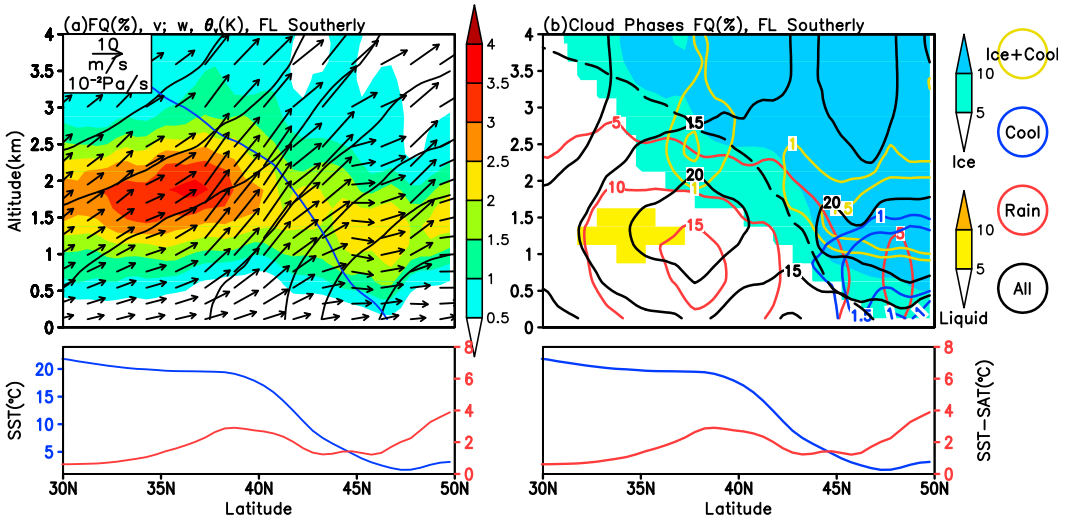

FIG. 9. As in Fig. 7, but for composites under southerly conditions.

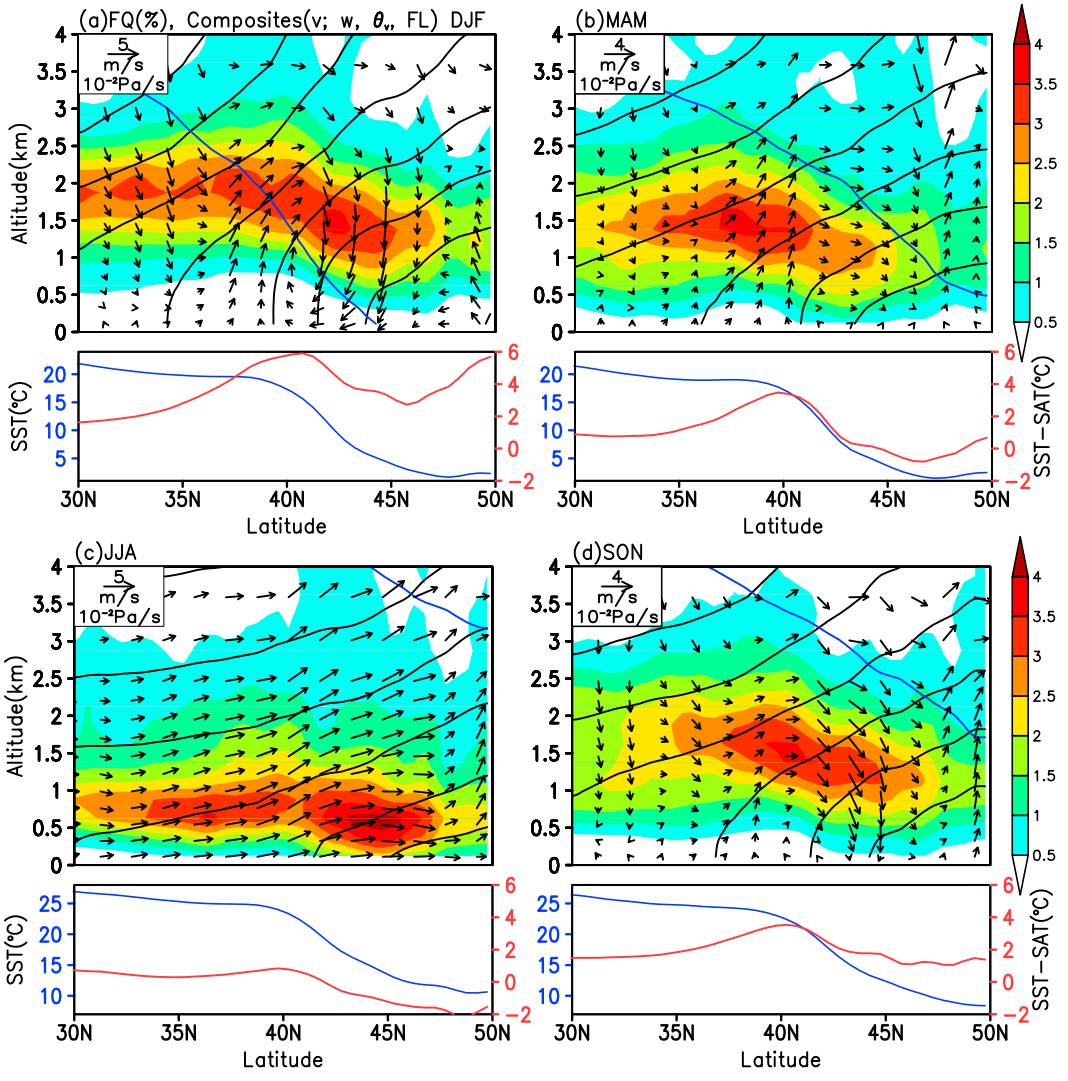

FIG. 10. (a) Repeated from Fig. 3b. (b)–(d) As in (a), but for March–May (MAM), June–August (JJA), and September–November (SON), respectively.

7. Summary and discussion

A sharp SST front develops between the warm Gulf Stream and cold continental shelf water during winter. We investigated the low-level cloud response to the SST front using *CALIPSO* and other high-resolution satellite observations and the ERA-Interim reanalysis. The results show a strong southward cross-frontal elevation of low-level clouds resulting from a secondary circulation within the MABL induced by the SST front.

The SST front exerts a strong influence on low-level clouds. Mean LCT averaged along *CALIPSO* tracks is lower than 1.4 km over the cold flank of the SST front but higher than 2.4 km over the Gulf Stream. In the zonal average, LCT over warm water is 0.5 km higher than over cold water. The SST front also influences the cross-frontal variations of cloud phase categories by affecting the freezing level. Rain is the prime form of precipitation over the Gulf Stream, ice clouds are dominant above the freezing level, and supercooled clouds are frequently observed above the MABL over the cold water in winter.

Our analysis supports the SLP adjustment mechanism proposed by Lindzen and Nigam (1987) as an explanation for the secondary circulation within the MABL induced by the SST front. The air temperature gradient within the MABL across the SST front results in surface convergence and ascending motion over the Gulf Stream, consequently deepening low-level clouds there.

The composite analysis shows that the cross-frontal transition of low-level clouds is more evident when surface winds are northerly. Stronger northerly winds

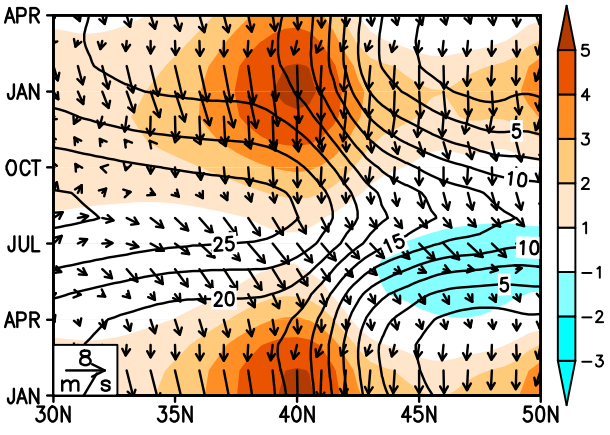

FIG. 11. Annual cycles of ERA-Interim SST (contours; °C), SST − SAT (color shading; °C), and surface winds (vectors) that are zonally averaged ERA-Interim fields along *CALIPSO* tracks. The horizontal and vertical components of the vectors represent the meridional and zonal surface winds, respectively.

bring cold air from the continent to the relatively warm ocean, leading to a well-mixed MABL that is deeper over the southern flank of the SST front. Furthermore, synoptic subsidence accompanying surface northerlies produces a strong inversion, thus setting up favorable condition for the formation of low-level clouds.

Norris and Iacobellis (2005) investigated how mid-tropospheric vertical velocity and advection over the SST gradient control midlatitude North Pacific cloud properties. They found that cumulus is prevalent under the conditions of synoptic descent and cold advection during winter and that the cloud breaks up as the MABL decouples when it is advected southward over the warmer water. Our results show that both the direction of surface meridional winds and the secondary circulation within the MABL induced by the SST front are important for the cross-frontal transition of low-level clouds. This is because the SST gradient in this study is much stronger than that in Norris and Iacobellis (2005).

Frequent and repeated observations by *CALIPSO* make the results reported here more reliable than case studies. Our results illustrate the utility of *CALIPSO* retrievals for air–sea interaction and MABL clouds in combination with AMSR-E and *CloudSat*. Further validation of the combined *CALIPSO* and *CloudSat* products (e.g., DARDAR) against in situ observations is desirable.

Acknowledgments. The authors wish to thank Dr. L.-F. Sheng for her valuable comments. This work was completed while JWL was a visiting student at IPRC and Scripps sponsored by the China Scholarship Council. The data used in this study are obtained from the atmospheric scientific data center of NASA (*CALIPSO*), the ICARE Thematic Center (DARDAR-MASK), Remote Sensing Systems (AMSR-E, QuikSCAT), the ECMWF data server (ERA-Interim), and the Global Energy and Water Cycle Exchanges Project (GPCP). This work is supported by the National Basic Research Program of China (2012CB955602), NASA, the Natural Science Foundation of China (41175006), and JAMSTEC. J. R. Norris was supported by NSF Award AGS-0946094.

REFERENCES

Bane, M., and E. Osgood, 1989: Wintertime air–sea interaction processes across the Gulf Stream. *J. Geophys. Res.,* **94,** 10 755–10 772, doi:10.1029/JC094iC08p10755.

Biswas, K. R., and P. V. Hobbs, 1990: Lightning over the Gulf Stream. *Geophys. Res. Lett.,* **17,** 941–943, doi:10.1029/GL017i007p00941.

Bouniol, D., F. Couvreux, P.-H. Kamsu-Tamo, M. Leplay, F. Guichard, F. Favot, and E. J. O'Connor, 2012: Diurnal and seasonal cycles of cloud occurrences, types, and radiative impact over West Africa. *J. Appl. Meteor. Climatol.,* **51,** 534–553, doi:10.1175/JAMC-D-11-051.1.

Caldwell, P., C. S. Bretherton, and R. Wood, 2005: Mixed-layer budget analysis of the diurnal cycle of entrainment in southeast Pacific stratocumulus. *J. Atmos. Sci.,* **62,** 3775–3791, doi:10.1175/JAS3561.1.

Chelton, D., M. Schlax, M. Freilich, and R. Milliff, 2004: Satellite measurements reveal persistent small-scale features in ocean winds. *Science,* **303,** 978–983.

Dee, D. P., and Coauthors, 2011: The ERA-Interim reanalysis: Configuration and performance of the data assimilation system. *Quart. J. Roy. Meteor. Soc.,* **137,** 553–597, doi:10.1002/qj.828.

Delanoë, J., and R. J. Hogan, 2008: A variational scheme for retrieving ice cloud properties from combined radar, lidar, and infrared radiometer. *J. Geophys. Res.,* **113,** D07204, doi:10.1029/2007JD009000.

——, and ——, 2010: Combined *CloudSat–CALIPSO*–MODIS retrievals of the properties of ice clouds. *J. Geophys. Res.,* **115,** D00H29, doi:10.1029/2009JD012346.

——, A. Protat, O. Jourdan, J. Pelon, M. Papazzoni, R. Dupuy, J.-F. Gayet, and C. Jouan, 2013: Comparison of airborne in situ, airborne radar–lidar, and spaceborne radar–lidar retrievals of polar ice cloud properties sampled during the POLARCAT campaign. *J. Atmos. Oceanic Technol.,* **30,** 57–73, doi:10.1175/JTECH-D-11-00200.1.

Hilburn, K. A., and F. J. Wentz, 2008: Intercalibrated passive microwave rain products from the unified microwave ocean retrieval algorithm (UMORA). *J. Appl. Meteor. Climatol.,* **47,** 778–794, doi:10.1175/2007JAMC1635.1.

Hobbs, P. V., 1987: The Gulf Stream rainband. *Geophys. Res. Lett.,* **14,** 1142–1145, doi:10.1029/GL014i011p01142.

Huang, C.-Y., and S. Raman, 1988: A numerical modeling study of the marine boundary layer over the Gulf Stream during cold air advection. *Bound.-Layer Meteor.,* **45,** 251–290, doi:10.1007/BF01066673.

Klein, S. A., and D. L. Hartmann, 1993: The seasonal cycle of low stratiform clouds. *J. Climate,* **6,** 1587–1606, doi:10.1175/1520-0442(1993)006<1587:TSCOLS>2.0.CO;2.

Li, M., and S. Zhang, 2013: Impact of sea surface temperature front on stratus-sea fog over the Yellow and East China Seas—A

case study with implications for climatology. *J. Ocean Univ. China,* **12,** 301–311, doi:10.1007/s11802-013-2218-5.

Li, X., W. Zheng, W. Pichel, C.-Z. Zou, P. Clemente-Colón, and K. S. Friedman, 2004: A cloud line over the Gulf Stream. *J. Geophys. Res.,* **31,** L14108, doi:10.1029/2004GL019892.

Lindzen, R., and S. Nigam, 1987: On the role of sea surface temperature gradients in forcing low-level winds and convergence in the tropics. *J. Atmos. Sci.,* **44,** 2418–2436, doi:10.1175/1520-0469(1987)044<2418:OTROSS>2.0.CO;2.

Liu, W. T., 2002: Progress in scatterometer application. *J. Oceanogr.,* **58,** 121–136, doi:10.1023/A:1015832919110.

Medeiros, B., L. Nuijens, C. Antoniazzi, and B. Stevens, 2010: Low-latitude boundary layer clouds as seen by *CALIPSO*. *J. Geophys. Res.,* **115,** D23207, doi:10.1029/2010JD014437.

Minobe, S., A. Kuwano-Yoshida, N. Komori, S.-P. Xie, and R. J. Small, 2008: Influence of the Gulf Stream on the troposphere. *Nature,* **452,** 206–209, doi:10.1038/nature06690.

——, M. Miyashita, A. Kuwano-Yoshida, H. Tokinaga, and S.-P. Xie, 2010: Atmospheric response to the Gulf Stream: Seasonal variations. *J. Climate,* **23,** 3699–3719, doi:10.1175/2010JCLI3359.1.

Nazaryan, H., M. P. McCormick, and W. P. Menzel, 2008: Global characterization of cirrus clouds using *CALIPSO* data. *J. Geophys. Res.,* **113,** D16211, doi:10.1029/2007JD009481.

Norris, J. R., 1998a: Low cloud type over the ocean from surface observations. Part I: Relationship to surface meteorology and the vertical distribution of temperature and moisture. *J. Climate,* **11,** 369–382, doi:10.1175/1520-0442(1998)011<0369:LCTOTO>2.0.CO;2.

——, 1998b: Low cloud type over the ocean from surface observations. Part II: Geographical and seasonal variations. *J. Climate,* **11,** 383–403, doi:10.1175/1520-0442(1998)011<0383:LCTOTO>2.0.CO;2.

——, and S. F. Iacobellis, 2005: North Pacific cloud feedbacks inferred from synoptic-scale dynamic and thermodynamic relationships. *J. Climate,* **18,** 4862–4878, doi:10.1175/JCLI3558.1.

O'Neill, L. W., D. B. Chelton, and S. K. Esbensen, 2010: The effects of SST-induced surface wind speed and direction gradients on midlatitude surface vorticity and divergence. *J. Climate,* **23,** 255–281, doi:10.1175/2009JCLI2613.1.

Sampe, T., and S.-P. Xie, 2007: Mapping high sea winds from space: A global climatology. *Bull. Amer. Meteor. Soc.,* **88,** 1965–1978, doi:10.1175/BAMS-88-12-1965.

Sanders, F., 1986: Explosive cyclogenesis in the west-central North Atlantic Ocean, 1981–84. Part I: Composite structure and mean behavior. *Mon. Wea. Rev.,* **114,** 1781–1794, doi:10.1175/1520-0493(1986)114<1781:ECITWC>2.0.CO;2.

——, and J. Gyakum, 1980: Synoptic-dynamic climatology of the ''bomb.'' *Mon. Wea. Rev.,* **108,** 1589–1606, doi:10.1175/1520-0493(1980)108<1589:SDCOT>2.0.CO;2.

Small, R. J., S.-P. Xie, and Y. Wang, 2003: Numerical simulation of atmospheric response to Pacific tropical instability waves. *J. Climate,* **16,** 3723–3741, doi:10.1175/1520-0442(2003)016<3723:NSOART>2.0.CO;2.

Stein, T. H. M., D. J. Parker, J. Delanoë, N. S. Dixon, R. J. Hogan, P. Knippertz, R. I. Maidment, and J. H. Marsham, 2011: The vertical cloud structure of the West African monsoon: A 4 year climatology using *CloudSat* and *CALIPSO*. *J. Geophys. Res.,* **116,** D22205, doi:10.1029/2011JD016029.

Tokinaga, H., Y. Tanimoto, S.-P. Xie, T. Sampe, H. Tomita, and H. Ichikawa, 2009: Ocean frontal effects on the vertical development of clouds over the western North Pacific: In situ and satellite observations. *J. Climate,* **22,** 4241–4260, doi:10.1175/2009JCLI2763.1.

Vaughan, M. A., and Coauthors, 2009: Fully automated detection of cloud and aerosol layers in the *CALIPSO* lidar measurements. *J. Atmos. Oceanic Technol.,* **26,** 2034–2050, doi:10.1175/2009JTECHA1228.1.

Wai, M. M.-K., and S. A. Stage, 1989: Dynamical analyses of marine atmospheric boundary layer structure near the Gulf Stream oceanic front. *Quart. J. Roy. Meteor. Soc.,* **115,** 29–44, doi:10.1002/qj.49711548503.

Winker, D. M., M. A. Vaughan, A. Omar, Y. Hu, K. A. Powell, Z. Liu, W. H. Hunt, and S. A. Young, 2009: Overview of the CALIPSO mission and CALIOP data processing algorithms. *J. Atmos. Oceanic Technol.,* **26,** 2310–2323, doi:10.1175/2009JTECHA1281.1.

Wood, R., 2012: Stratocumulus clouds. *Mon. Wea. Rev.,* **140,** 2373–2423, doi:10.1175/MWR-D-11-00121.1.

Young, G. S., and T. D. Sikora, 2003: Mesoscale stratocumulus bands caused by Gulf Stream meanders. *Mon. Wea. Rev.,* **131,** 2177–2191, doi:10.1175/1520-0493(2003)131<2177:MSBCBG>2.0.CO;2.

Zhang, C., Y. Wang, A. Lauer, K. Hamilton, and F. Xie, 2012: Cloud base and top heights in the Hawaiian region determined with satellite and ground-based measurements. *Geophys. Res. Lett.,* **39,** L15706, doi:10.1029/2012GL052355.